Physics Letters B 811 (2020) 135986

Contents lists available at ScienceDirect

Physics Letters B

www.elsevier.com/locate/physletb

An extended $R^{(2)}_{\Psi_m}(\Delta S_2)$ correlator for detecting and characterizing the Chiral Magnetic Wave

Niseem Magdy [a], Mao-Wu Nie [b,c], Ling Huang [d,e,f], Guo-Liang Ma [d,f], Roy A. Lacey [g,*]

[a] Department of Physics, University of Illinois at Chicago, Chicago, IL 60607, USA
[b] Institute of Frontier and Interdisciplinary Science, Shandong University, Qingdao, Shandong, 266237, China
[c] Key Laboratory of Particle Physics and Particle Irradiation, Ministry of Education, Shandong University, Qingdao, Shandong, 266237, China
[d] Shanghai Institute of Applied Physics, Chinese Academy of Sciences, Shanghai 201800, China
[e] University of Chinese Academy of Sciences, Beijing 100049, China
[f] Key Laboratory of Nuclear Physics and Ion-beam Application (MOE), Institute of Modern Physics, Fudan University, Shanghai 200433, China
[g] Depts. of Chemistry & Physics, Stony Brook University, Stony Brook, NY 11794, USA

ARTICLE INFO

Article history:
Received 7 May 2020
Received in revised form 23 October 2020
Accepted 24 November 2020
Available online 30 November 2020
Editor: D.F. Geesaman

ABSTRACT

The extended $R^{(2)}_{\Psi_m}(\Delta S_2)$ correlator is presented and examined for its efficacy to detect and characterize the quadrupole charge separation (ΔS_2) associated with the purported Chiral Magnetic Wave (CMW) produced in heavy-ion collisions. Sensitivity tests involving varying degrees of charge separation injected into events simulated with the Multi-Phase Transport Model (AMPT) show that the $R^{(2)}_{\Psi_m}(\Delta S_2)$ correlators provide discernible responses for the background- and signal-driven quadrupole charge separation. This distinction could help identify CMW-induced quadrupole charge separation via measurements of the $R^{(2)}_{\Psi_2}(\Delta S_2)$ and $R^{(2)}_{\Psi_3}(\Delta S_2)$ correlators, relative to the second- (Ψ_2) and third-order (Ψ_3) event planes. The tests also indicate a sensitivity level that would allow for robust experimental characterization of possible CMW-induced charge separation.

Heavy-ion collisions at the Relativistic Heavy Ion Collider (RHIC) and the Large Hadron Collider (LHC) can lead to a magnetized chiral relativistic quark-gluon plasma (QGP) [1–5], in which the mass of fermions is negligible compared to the temperature and/or chemical potential. Such a plasma, which is akin to the primordial plasma in the early Universe [6,7] and several types of degenerate forms of matter in compact stars [8], have pseudo-relativistic analogs in Dirac and Weyl materials [9–11]. It is further characterized not only by an exactly conserved electric charge but also by an approximately conserved chiral charge, violated only by the quantum chiral anomaly [12,13].

The study of anomalous transport in magnetized chiral plasmas can give fundamental insight not only on the complex interplay of chiral symmetry restoration, axial anomaly and gluon topology in the QGP [5,14–17], but also on the evolution of magnetic fields in the early Universe [18,19]. Two of the principal anomalous processes in these plasmas [for electric and chiral charge chemical potential $\mu_{V,A} \neq 0$] are the chiral separation effect (CSE) [20–22] and the chiral magnetic effect (CME) [23]. The CSE is derived from the induction of a non-dissipative chiral axial current:

$$\vec{J}_A = \frac{N_c e \vec{B}}{2\pi^2}\mu_V, \text{for}\, \mu_V \neq 0, \tag{1}$$

where N_c is the color factor, μ_V is the vector (electric) chemical potential and $\vec{B}$ is the magnetic field. The CME is similarly characterized by the vector current:

$$\vec{J}_V = \frac{N_c e \vec{B}}{2\pi^2}\mu_A, \text{for}\, \mu_A \neq 0, \tag{2}$$

where μ_A is the axial chemical potential that quantifies the axial charge asymmetry or imbalance between right- and left-handed quarks in the plasma [22–25].

The interplay between the CSE and CME in the QGP produced in heavy ion collisions, can lead to the production of a gapless collective mode – termed the chiral magnetic wave (CMW) [26], stemming from the coupling between the density waves of the electric and chiral charges. The propagation of the CMW is sustained by alternating oscillations of the local electric and chiral charge den-

* Corresponding author.
E-mail addresses: niseemm@gmail.com (N. Magdy), glma@fudan.edu.cn (G.-L. Ma), Roy.Lacey@stonybrook.edu (R.A. Lacey).

https://doi.org/10.1016/j.physletb.2020.135986

sities that feed into each other to ultimately transport positive (negative) charges out-of-plane and negative (positive) charges in-plane to form an electric quadrupole. Here, the reaction plane $\Psi_{\rm RP}$, is defined by the impact vector $\vec{b}$ and the beam direction, so the poles of the quadrupole lie along the direction of the $\vec{B}$-field (out-of-plane) which is essentially perpendicular to $\Psi_{\rm RP}$.

The electric charge quadrupole can induce charge-dependent quadrupole correlations between the positively- and negatively-charged particles produced in the collisions [2,4,5,26–29]. Such correlations can be measured with suitable correlators to aid full characterization of the CMW.

A pervasive approach employed in prior, as well as ongoing experimental studies of the CMW, is to measure the elliptic- or quadrupole flow difference between negatively- and positively charged particles [30,31]:

$$\Delta v_2 \equiv v_2^- - v_2^+ \simeq r A_{\rm ch}, \quad A_{\rm ch} = \frac{(N^+ - N^-)}{(N^+ + N^-)} \tag{3}$$

as a function of charge asymmetry $A_{\rm ch}$. Here, $N^{\pm}$ denotes the number of positively- (negatively-) charged hadrons measured in a given event; the slope parameter r, which is experimentally determined from the measurements, is purported to give an estimate of the strength of the CMW signal [2,4,5,26,29,32,33]. However, a wealth of measurements reported by the ALICE [32,33], CMS [34,35] and STAR [36,37] collaborations, highlight a significant influence from the effects of background, suggesting a need for supplemental measurements with improved correlators that not only suppress background, but are also sensitive to small CMW-driven signals in the presence of these backgrounds.

In prior work, we have proposed [38] and validated the utility [39–41] of the $R_{\Psi_m}(\Delta S)$ correlator for robust detection and characterization of the CME-driven dipole charge separation relative to the $\Psi_{2,3}$ planes. Here, we follow the lead of Ref. [42] by first, extending the correlator for study of the CMW-driven quadrupole charge separation, followed by detailed sensitivity tests of the correlator with the aid of AMPT model simulations.

The extended correlators, $R^{(d)}_{\Psi_m}(\Delta S_d)$, are constructed for each event plane Ψ_m, as the ratio:

$$R^{(d)}_{\Psi_m}(\Delta S_d) = C^{\parallel}_{\Psi_m}(\Delta S_d)/C^{\perp}_{\Psi_m}(\Delta S_d),\ m = 2, 3, \tag{4}$$

where $d = 1$ and 2 denote dipole and quadrupole charge separation respectively, and $C^{\parallel}_{\Psi_m}(\Delta S_d)$ and $C^{\perp}_{\Psi_m}(\Delta S_d)$ are correlation functions designed to quantify the dipole and quadrupole charge separation ΔS_d, parallel and perpendicular (respectively) to the $\vec{B}$-field, i.e., approximately perpendicular and parallel (respectively) to $\Psi_{\rm RP}$.

The correlation functions used to quantify the dipole and quadrupole charge separation parallel to the $\vec{B}$-field, are constructed from the ratio of two distributions:

$$C^{\parallel}_{\Psi_m}(\Delta S_d) = \frac{N_{\rm real}(\Delta S_d)}{N_{\rm Shuffled}(\Delta S_d)},\ m = 2, 3, \tag{5}$$

where $N_{\rm real}(\Delta S_d)$ is the distribution over events, of charge separation relative to the Ψ_m planes in each event:

$$\Delta S_d = \frac{\sum_1^{n^+} w_i^+ \sin(\frac{md}{2}\Delta\varphi_m)}{\sum_1^{n^+} w_i^+} - \frac{\sum_1^{n^-} w_i^- \sin(\frac{md}{2}\Delta\varphi_m)}{\sum_1^{n^-} w_i^-}, \tag{6}$$

where n^- and n^+ are the numbers of negatively and positively charged particles emitted about the estimated Ψ_m planes, $w_i^{\pm}$ are charge-dependent weights which take account of the azimuthal acceptance of the charged particles and $\Delta\varphi_m = \phi - \Psi_m$. The $N_{\rm Shuffled}(\Delta S_d)$ distribution is similarly obtained from the same events, following random reassignment (shuffling) of the charge of each particle in an event. This procedure ensures identical properties for the numerator and the denominator in Eq. (5), except for the charge-dependent correlations which are of interest.

The correlation functions $C^{\perp}_{\Psi_m}(\Delta S_d)$, used to quantify the dipole and quadrupole charge separation perpendicular to the $\vec{B}$-field, are constructed with the same procedure outlined for $C_{\Psi_m}(\Delta S_d)$, but with Ψ_m replaced by $\Psi_m + \pi/md$. Note that this rotation of Ψ_m maps the sine terms in Eq. (6) into cosine terms.

The correlators $R^{(d)}_{\Psi_m}(\Delta S_d) = C^{\parallel}_{\Psi_2}(\Delta S_d)/C^{\perp}_{\Psi_m}(\Delta S_d)$, are only sensitive to charge dependent effects, because the numerator and denominator of the requisite correlation functions are the same, except for charge shuffling (cf. Eq. (5)). The correlation function $C^{\parallel}_{\Psi_2}(\Delta S_d)$ measures charge separation along the direction of the $\vec{B}$-field (signal + background) while $C^{\perp}_{\Psi_m}(\Delta S_d)$ measures charge separation perpendicular to the $\vec{B}$-field (background only). Therefore, one expects significant suppression of the background via the ratio $C^{\parallel}_{\Psi_2}(\Delta S_d)/C^{\perp}_{\Psi_m}(\Delta S_d) = R^{(d)}_{\Psi_m}(\Delta S_d)$. For charge-sensitive backgrounds such as local charge conservation, and resonance decays coupled to flow, the correlator leverages the difference between $R^{(d)}_{\Psi_2}(\Delta S_d)$ and $R^{(d)}_{\Psi_3}(\Delta S_d)$ to discern between signal and background because $R^{(d)}_{\Psi_3}(\Delta S_d)$ only measures background. Note that the CME- and CMW-driven charge separations are strongly correlated with the $\vec{B}$-field, which is essentially uncorrelated with the orientation of the Ψ_3 plane. Thus, if the background predominates, $R^{(d)}_{\Psi_2}(\Delta S_d)$ and $R^{(d)}_{\Psi_3}(\Delta S_d)$ should show similar magnitudes and trends. For small systems such as $p/d/^3$He+Au and p+Pb, a similar insensitivity to the $\vec{B}$-field is expected for $R^{(d)}_{\Psi_2}(\Delta S_d)$ [akin to that for $R^{(d)}_{\Psi_3}(\Delta S_d)$], due to the weak correlation between the $\vec{B}$-field and the Ψ_2 planes for these systems.

The response and the sensitivity of the $R^{(1)}_{\Psi_2}(\Delta S_1)$ correlator to CME-driven charge separation is detailed in Refs. [38,41]. For CMW-driven charge separation, $R^{(2)}_{\Psi_2}(\Delta S_2)$ is expected to show an approximately linear dependence on ΔS_2 for $|\Delta S_2| \lesssim 3$, due to a shift in the mean of the distributions for $C^{\perp}_{\Psi_2}(\Delta S_2)$ relative to $C^{\parallel}_{\Psi_2}(\Delta S_2)$, induced by the quadrupole charge separation (cf. Fig. 1 and later discussions). Thus, the slope of the plot of $R^{(2)}_{\Psi_2}(\Delta S_2)$ vs. ΔS_2, encodes the magnitude of the quadrupole charge separation signal. This slope is also influenced by particle number fluctuations and the resolution of the Ψ_2 plane which fluctuates about $\Psi_{\rm RP}$. The influence of the particle number fluctuations can be minimized by scaling ΔS_2 by the width $\sigma_{\Delta S_{\rm h}}$ of the distribution for $N_{\rm shuffled}(\Delta S_2)$ *i.e.*, $\Delta S_2' = \Delta S_2/\sigma_{\Delta S_{\rm h}}$. Similarly, the effects of the event plane resolution can be accounted for by scaling $\Delta S_2'$ by the resolution factor $\delta_{\rm Res}$, *i.e.*, $\Delta S_2'' = \Delta S_2'\delta_{\rm Res}$, where $\delta_{\rm Res}$ is the event plane resolution. The efficacy of these scaling procedures has been confirmed via detailed data-driven studies involving both simulated and experimental data.

Our sensitivity studies for $R^{(2)}_{\Psi_m}(\Delta S_2)$, relative to the Ψ_2 and Ψ_3 event planes, are performed with AMPT events in which varying degrees of proxy CMW-driven quadrupole charge separation were introduced [42,43]. The version of the model used gives a good representation of the experimentally measured particle yields, spectra, flow, etc., [44–49]; it incorporates important charge separation backgrounds such as local charge conservation and resonance decays coupled to collective flow. Therefore, it provides a good estimate of both the magnitude and the properties of the background-driven quadrupole charge separation expected in the data collected at RHIC and the LHC.

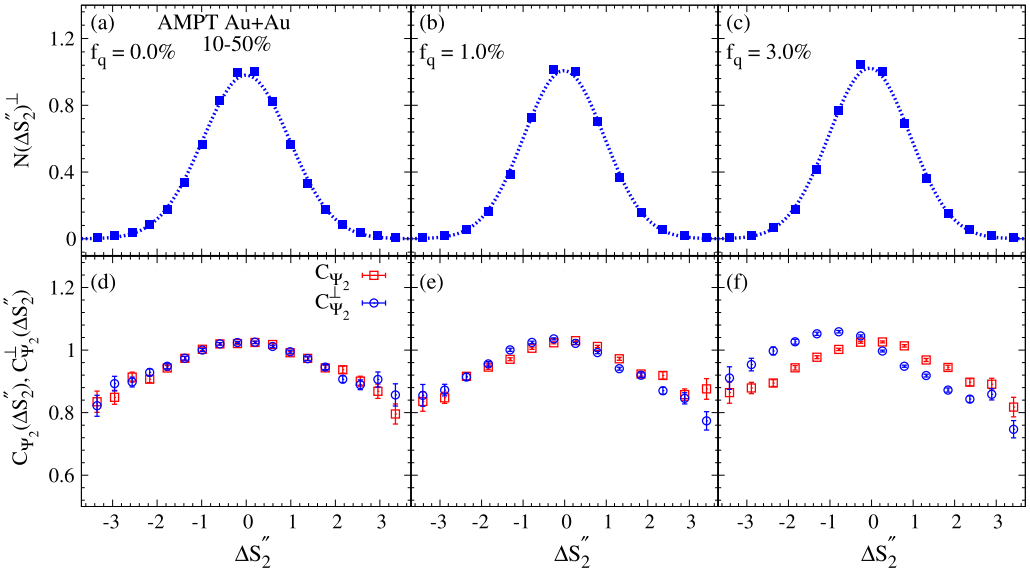

Fig. 1. Simulated $N(\Delta S_2'')^{\perp}$ distributions (with respect to Ψ_2) for several input values of quadrupole charge separation characterized by f_q (a-c); comparison of the $C^{\parallel}_{\Psi_2}(\Delta S_2'')$ and $C^{\perp}_{\Psi_2}(\Delta S_2'')$ correlation functions for the same values of f_q (d-f). The simulated results are for 10-50% Au+Au collisions at $\sqrt{s_{\rm NN}}$ = 200 GeV.

We simulated Au+Au collisions at $\sqrt{s_{\rm NN}}$ = 200 GeV with the same AMPT model version used in our prior studies [40–42]; this version incorporates both string melting and local charge conservation. In brief, the model follows four primary stages: (i) an initial-state, (ii) a parton cascade phase, (iii) a hadronization phase in which partons are converted to hadrons, and (iv) a hadronic re-scattering phase. The initial-state essentially simulates the spatial and momentum distributions of mini-jet partons from QCD hard processes and soft string excitations as encoded in the HIJING model [50,51]. The parton cascade considers the strong interactions among partons via elastic partonic collisions [52]. Hadronization is simulated via a coalescence mechanism. After hadronization, the ART model is invoked to simulate baryon-baryon, baryon-meson and meson-meson interactions [53].

A formal mechanism for generation of the CMW is not implemented in the AMPT model. However, a proxy CMW-induced quadrupole charge separation can be implemented [43,54] by interchanging the position coordinates (x, y, z) for a fraction (f_q) of the in-plane light quarks (u, d and s) carrying positive (negative) charges with out-of-plane quarks carrying negative (positive) charges, at the start of the partonic stage. This procedure lends itself to two quadrupole charge configurations, relative to the in-plane and out-of-plane orientations. The first or Type (I), is for events with negative net charge ($A_{\rm ch} < -0.01$) in which the u and $\bar{d}$ are set to be concentrated on the equator of the quadrupole (in-plane), while d and $\bar{u}$ quarks are set to be concentrated at the poles of the quadrupole (out-of-plane). The second or Type (II), is for events with positive net charge ($A_{\rm ch} > -0.01$) in which the in-plane and out-of-plane quark configurations are swapped. The latter configuration was employed for the bulk of the AMPT events generated with the proxy input signals. The magnitude of these signals is set by the fraction f_q, which serves to characterize the strength of the quadrupole charge separation.

The AMPT events with varying degrees of quadrupole signals were analyzed with the $R^{(2)}_{\Psi_{2,3}}(\Delta S_2)$ correlators to identify and quantify their response to the respective input signals. The analysis included charged particles with $|\eta| < 1.0$ and transverse momentum $0.2 < p_T < 2$ GeV/c. To enhance the statistical significance of the measurements, the participant plane Ψ_m was determined with charged hadrons in the range $2.5 < \eta < 4.0$. The quadrupole charge separation of charged hadrons in $|\eta| < 1.0$ were then measured relative to Ψ_m and corrected for particle number fluctuations ($\Delta S_2' = \Delta S_2/\sigma_{\Delta_{\rm Sh}}$) and event-plane resolution ($\Delta S_2'' = \Delta S_2'\delta_{\rm Res}$), as described earlier.

The top panels of Fig. 1 confirm the Gaussian distributions for $N(\Delta S_2'')^{\perp}$ as expected from the central limit theorem. They also indicate a shift in the mean value as f_q increases; the mean value is $\sim$ zero for $f_q = 0$ (a) and progressively shifts to $\Delta S_2'' < 0$ for $f_q > 0$ (b and c). These shifts reflect the charge-dependent v_2 [cf. Eq. (6) for $\Psi_m + \pi/md$] which results from an interchange of the position coordinates for a fraction (f_q) of the in-plane light quarks/anti-quarks carrying negative charges with out-of-plane quarks/anti-quarks carrying positive charges, at the start of the partonic stage in the AMPT model. These signal-induced shifts for $f_q > 0$, are made more transparent in Figs. 1 (d)-(f) where the shift of $C^{\perp}_{\Psi_2}(\Delta S_2'')$ relative to the $C^{\parallel}_{\Psi_2}(\Delta S_2'')$ correlation function is apparent cf. Fig. 1 (f).

The $R^{(2)}_{\Psi_2}(\Delta S_2'')$ and $R^{(2)}_{\Psi_3}(\Delta S_2'')$ correlators, obtained for several input values of f_q, are shown in Fig. 2. They indicate an essentially flat distribution for $R^{(2)}_{\Psi_3}(\Delta S_2'')$ irrespective of the value of f_q. These patterns are consistent with the expected insensitivity of $R^{(2)}_{\Psi_3}(\Delta S_2'')$ to CMW-driven charge separation due to the absence of a strong correlation between the $\vec{B}$-field and the orientation of the Ψ_3 plane. Figs. 2 (a)-(f) show that the $R^{(2)}_{\Psi_2}(\Delta S_2'')$ correlator evolves from a flat distribution for $f_q = 0$, to an approximately linear dependence on $\Delta S_2''$ (for $|\Delta S_2''| \lesssim 3$) with slopes that reflect the increase in the magnitude of the input CMW-driven charge separation with f_q. These patterns not only confirm the input quadrupole charge separation signal in each case; they suggest that the $R^{(2)}_{\Psi_m}(\Delta S_2)$ correlator is relatively insensitive to a possible $v_{2,3}$-driven background [and their associated fluctuations] as well as the local charge conservation effects implemented in the AMPT model. Note the essentially flat distributions for $R^{(2)}_{\Psi_3}(\Delta S_2'')$ and for $R^{(2)}_{\Psi_2}(\Delta S_2'')$ when the input signal is set to zero.

This insensitivity can be further checked via the event-shape engineering, through fractional cuts on the distribution of the magnitude of the q_2 flow vector [55]. Here, the underlying notion is that elliptic flow v_2, which is a major driver of background correlations, is strongly correlated with q_2 [56,57]. Thus, the magnitude of the background correlations can be increased (decreased) by selecting events with larger (smaller) q_2 values. Such selections were

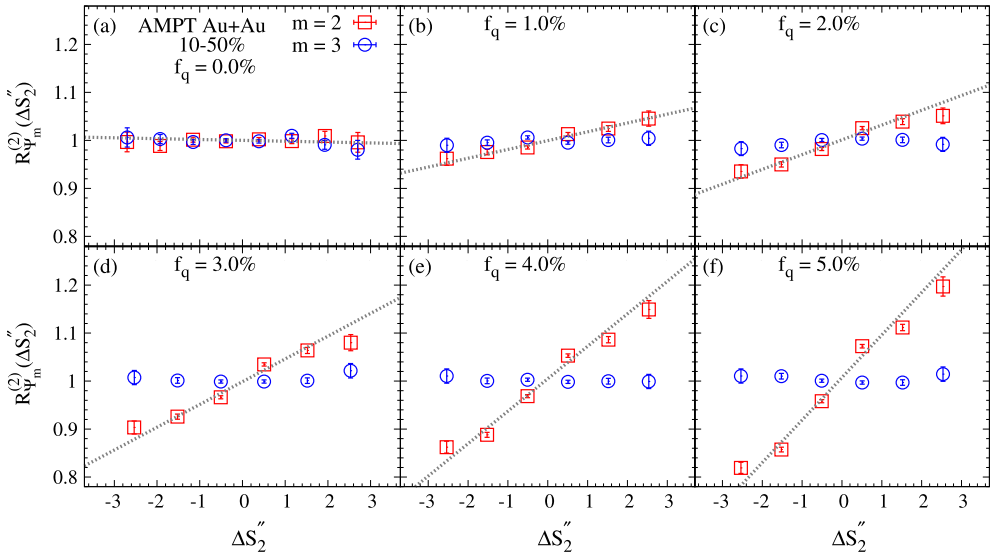

Fig. 2. $R^{(2)}_{\Psi_m}(\Delta S_2)$ vs. $\Delta S''$ for several input values of quadrupole charge separation characterized by f_q, for 10-50% Au+Au collisions ($\sqrt{s_{\rm NN}}$ = 200 GeV).

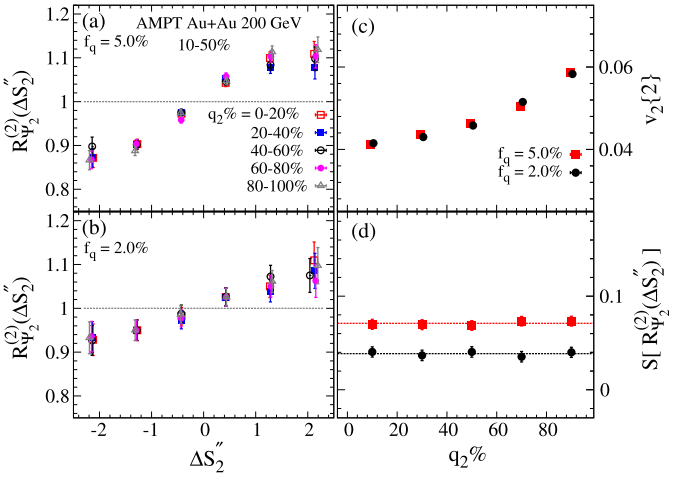

Fig. 3. Comparison of the simulated $R^{(2)}_{\Psi_2}(\Delta S_2'')$ correlators for q_2 selected events in 10 − 50% central, Au+Au collisions at $\sqrt{s_{\rm NN}} = 200$ GeV for $f_q = 5.0\%$ (a) and $f_q = 2.0\%$ (b). The right panels show comparisons for $v_2(q_2)$ (c) and the slopes extracted from the $R^{(2)}_{\Psi_2}$ vs. $\Delta S_2''$ distributions (d) shown in panel (a) and (b); the dotted lines represent fits to the simulated data.

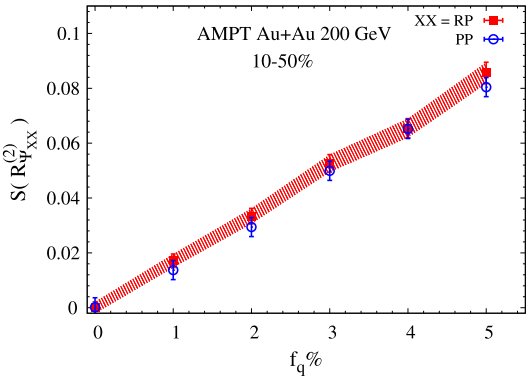

Fig. 4. f_q dependence of the slopes extracted from the $R^{(2)}_{\Psi_2}(\Delta S_2'')$ vs. $\Delta S_2''$ distributions. Results are shown for 10-50% central Au+Au ($\sqrt{s_{\rm NN}}$ = 200 GeV) AMPT events.

made by splitting each event into three sub-events; $A[\eta < -0.3]$, $B[|\eta| < 0.3]$, and $C[\eta > 0.3]$, where sub-event B was used to evaluate q_2, and the other sub-events used to evaluate $R^{(2)}_{\Psi_2}(\Delta S_2'')$ via the methods described earlier.

Fig. 3 shows a comparison of the q_2-selected $R^{(2)}_{\Psi_2}$ distributions (a) and (b), v_2 (c) and the slopes (d) extracted from the distributions shown in panels (a) and (b), respectively. These results were obtained for 10-50% central Au+Au collisions with f_q=5% and f_q=2%. They indicate that while v_2 increases with q_2, the corresponding slope for the $R^{(2)}_{\Psi_2}$ correlators (Fig. 3 (c)) show little, if any, change. This insensitivity to the value of q_2 is incompatible with a dominating influence of background-driven contributions to $R^{(2)}_{\Psi_2}(\Delta S_2'')$. It is noteworthy that a further analysis performed for background-driven charge separation with strong local charge conservation, also indicated that $R^{(2)}_{\Psi_2}(\Delta S_2'')$ is essentially insensitive to this background.

The $R^{(2)}_{\Psi_2}(\Delta S_2'')$ distributions shown in Fig. 2, indicate slopes that visibly increase with f_q. To quantify the measured signal strengths, we extracted the slope S, of the respective $R^{(2)}_{\Psi_2}(\Delta S_2'')$ distributions shown in the figure. Fig. 4 indicates a linear dependence of these slopes on f_q with little, if any, intercept. It also shows that the magnitude and trends of S are independent of the event plane used in the analysis. These results suggest that the $R^{(2)}_{\Psi_2}$ correlator not only suppresses background but would be sensitive to small CMW-driven quadrupole charge separation in the presence of a background.

The slopes S, of the $R^{(2)}_{\Psi_2}(\Delta S_2'')$ vs. $\Delta S_2''$ distributions can also be explored as a function of the charge asymmetry $A_{\rm ch}$ as shown in Fig. 5 for $f_q = 5.0\%$ and $f_q = 2.0\%$. Here, the $A_{\rm ch}$ distribution shown in the inset, hints at the fact that the model parameters used in the AMPT simulations were chosen to give a positive net charge, when averaged over all events. Fig. 5 shows the expected decrease of S with $A_{\rm ch}$ for $A_{\rm ch} < 0$, with a rate which depends on the magnitude of f_q. It also shows that the sign of S can even be flipped for sufficiently large negative values of $A_{\rm ch}$, in accord with expectations. Fig. 5 also shows that the slopes for $R^{(2)}_{\Psi_3}(\Delta S_2'')$ vs. $\Delta S_2''$ are insensitive to $A_{\rm ch}$ as might be expected. These dependencies could serve as further aids to CMW signal detection and characterization in future experimental measurements.

In summary, we have extended the $R^{(1)}_{\Psi_m}(\Delta S_1)$ correlator, previously used to measure CME-induced dipole charge separation, to include the $R^{(2)}_{\Psi_m}(\Delta S_2)$ correlator, which can be used to measure CMW-driven quadrupole charge separation. Validation tests involving varying degrees of quadrupole charge separation (sig-

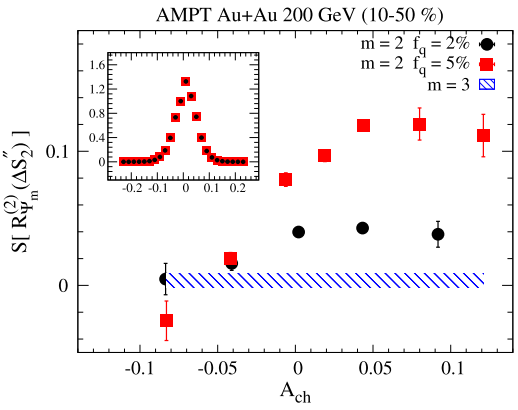

Fig. 5. $A_{\rm ch}$ dependence of the slopes extracted from the $R^{(2)}_{\Psi_2}(\Delta S''_2)$ vs. $\Delta S''_2$ distributions for different $A_{\rm ch}$ selections for $f_q = 5.0\%$ and $f_q = 2.0\%$. The inset shows normalized distributions for $A_{\rm ch}$. Results are shown for 10-50% central Au+Au ($\sqrt{s_{\rm NN}}$ = 200 GeV) AMPT events.

nal) injected into AMPT events, show that the $R^{(2)}_{\Psi_m}(\Delta S_2)$ correlator provides discernible responses for background- and signal-driven charge separation which could aid robust identification of the CMW. They also indicate a level of sensitivity that would allow for precise experimental characterization of the purported CMW-driven quadrupole charge separation via $R^{(2)}_{\Psi_m}(\Delta S_2)$ measurements in heavy-ion collisions.

Declaration of competing interest

The authors declare that they have no known competing financial interests or personal relationships that could have appeared to influence the work reported in this paper.

Acknowledgements

This research is supported by the US Department of Energy, Office of Science, Office of Nuclear Physics, under contracts DE-FG02-87ER40331.A008 (RL), DE-FG02-94ER40865 (NM) and by the National Natural Science Foundation of China under Grants No. 11890714, No. 11835002, No. 11961131011, No. 11421505, the Key Research Program of the Chinese Academy of Sciences under Grant No. XDPB09 (L.H. and G.-L.M.)

References

[1] Dmitri Kharzeev, Parity violation in hot QCD: why it can happen, and how to look for it, Phys. Lett. B 633 (2006) 260–264, arXiv:hep-ph/0406125.
[2] Jinfeng Liao, Anomalous transport effects and possible environmental symmetry 'violation' in heavy-ion collisions, Pramana 84 (2015) 901–926, arXiv:1401.2500 [hep-ph].
[3] Vladimir A. Miransky, Igor A. Shovkovy, Quantum field theory in a magnetic field: from quantum chromodynamics to graphene and Dirac semimetals, Phys. Rep. 576 (2015) 1–209, arXiv:1503.00732 [hep-ph].
[4] Xu-Guang Huang, Electromagnetic fields and anomalous transports in heavy-ion collisions — a pedagogical review, Rep. Prog. Phys. 79 (2016) 076302, arXiv:1509.04073 [nucl-th].
[5] D.E. Kharzeev, J. Liao, S.A. Voloshin, G. Wang, Chiral magnetic and vortical effects in high-energy nuclear collisions—a status report, Prog. Part. Nucl. Phys. 88 (2016) 1–28, arXiv:1511.04050 [hep-ph].
[6] Igor Rogachevskii, Oleg Ruchayskiy, Alexey Boyarsky, Jürg Fröhlich, Nathan Kleeorin, Axel Brandenburg, Jennifer Schober, Laminar and turbulent dynamos in chiral magnetohydrodynamics-I: theory, Astrophys. J. 846 (2017) 153, arXiv:1705.00378 [physics.plasm-ph].
[7] Valery A. Rubakov, Dmitry S. Gorbunov, Introduction to the Theory of the Early Universe, World Scientific, Singapore, 2017.
[8] Fridolin Weber, Strange quark matter and compact stars, Prog. Part. Nucl. Phys. 54 (2005) 193–288, arXiv:astro-ph/0407155 [astro-ph].
[9] Oskar Vafek, Ashvin Vishwanath, Dirac fermions in solids: from high-Tc cuprates and graphene to topological insulators and Weyl semimetals, Annu. Rev. Condens. Matter Phys. 5 (2014) 83–112, arXiv:1306.2272 [cond-mat.mes-hall].
[10] A.A. Burkov, Chiral anomaly and transport in Weyl metals, J. Phys. Condens. Matter 27 (2015) 113201, arXiv:1502.07609 [cond-mat.mes-hall].
[11] E.V. Gorbar, V.A. Miransky, I.A. Shovkovy, P.O. Sukhachov, Anomalous transport properties of Dirac and Weyl semimetals (review article), Low Temp. Phys. 44 (2018) 487–505, Fiz. Nizk. Temp. 44 (2017) 635, arXiv:1712.08947 [cond-mat.mes-hall].
[12] Stephen L. Adler, Axial vector vertex in spinor electrodynamics, Phys. Rev. 177 (1969) 2426–2438, [,241(1969)].
[13] J.S. Bell, R. Jackiw, A PCAC puzzle: $\pi^0 \to \gamma\gamma$ in the σ model, Nuovo Cimento A 60 (1969) 47–61.
[14] Guy D. Moore, Marcus Tassler, The sphaleron rate in SU(N) gauge theory, J. High Energy Phys. 02 (2011) 105, arXiv:1011.1167 [hep-ph].
[15] M. Mace, S. Schlichting, R. Venugopalan, Off-equilibrium sphaleron transitions in the Glasma, Phys. Rev. D 93 (2016) 074036, arXiv:1601.07342 [hep-ph].
[16] Jinfeng Liao, Volker Koch, Adam Bzdak, On the charge separation effect in relativistic heavy ion collisions, Phys. Rev. C 82 (2010) 054902, arXiv:1005.5380 [nucl-th].
[17] Volker Koch, Soeren Schlichting, Vladimir Skokov, Paul Sorensen, Jim Thomas, Sergei Voloshin, Gang Wang, Ho-Ung Yee, Status of the chiral magnetic effect and collisions of isobars, Chin. Phys. C 41 (2017) 072001, arXiv:1608.00982 [nucl-th].
[18] M. Joyce, Mikhail E. Shaposhnikov, Primordial magnetic fields, right-handed electrons, and the Abelian anomaly, Phys. Rev. Lett. 79 (1997) 1193–1196, arXiv:astro-ph/9703005 [astro-ph].
[19] Hiroyuki Tashiro, Tanmay Vachaspati, Alexander Vilenkin, Chiral effects and cosmic magnetic fields, Phys. Rev. D 86 (2012) 105033, arXiv:1206.5549 [astro-ph.CO].
[20] A. Vilenkin, Equilibrium parity violating current in a magnetic field, Phys. Rev. D 22 (1980) 3080–3084.
[21] Max A. Metlitski, Ariel R. Zhitnitsky, Anomalous axion interactions and topological currents in dense matter, Phys. Rev. D 72 (2005) 045011, arXiv:hep-ph/0505072 [hep-ph].
[22] Dam T. Son, Piotr Surowka, Hydrodynamics with triangle anomalies, Phys. Rev. Lett. 103 (2009) 191601, arXiv:0906.5044 [hep-th].
[23] Kenji Fukushima, Dmitri E. Kharzeev, Harmen J. Warringa, The chiral magnetic effect, Phys. Rev. D 78 (2008) 074033, arXiv:0808.3382 [hep-ph].
[24] Valentin I. Zakharov, Chiral magnetic effect in hydrodynamic approximation, Lect. Notes Phys. 871 (2012) 295, https://doi.org/10.1007/978-3-642-37305-3-11, arXiv:1210.2186 [hep-ph], 2013.
[25] Kenji Fukushima, Views of the chiral magnetic effect, Lect. Notes Phys. 871 (2013) 241–259, arXiv:1209.5064 [hep-ph].
[26] Dmitri E. Kharzeev, Ho-Ung Yee, Chiral magnetic wave, Phys. Rev. D 83 (2011) 085007, arXiv:1012.6026 [hep-th].
[27] Stephanov Mikhail, Ho-Ung Yee, Charged elliptic flow at zero charge asymmetry, Phys. Rev. C 88 (2013) 014908, arXiv:1304.6410 [nucl-th].
[28] Zhang-Zhu Han, Jun Xu, Charge asymmetry dependence of the elliptic flow splitting in relativistic heavy-ion collisions, Phys. Rev. C 99 (2019) 044915, arXiv:1904.03544 [nucl-th].
[29] Xin-Li Zhao, Guo-Liang Ma, Yu-Gang Ma, Novel mechanism for electric quadrupole moment generation in relativistic heavy-ion collisions, Phys. Lett. B 792 (2019) 413–418, arXiv:1901.04156 [hep-ph].
[30] Yannis Burnier, Dmitri E. Kharzeev, Jinfeng Liao, Ho-Ung Yee, Chiral magnetic wave at finite baryon density and the electric quadrupole moment of quark-gluon plasma in heavy ion collisions, Phys. Rev. Lett. 107 (2011) 052303, arXiv:1103.1307 [hep-ph].
[31] Y. Burnier, D.E. Kharzeev, J. Liao, H.U. Yee, From the chiral magnetic wave to the charge dependence of elliptic flow, arXiv:1208.2537 [hep-ph], 2012.
[32] Sergei A. Voloshin, Ronald Belmont, Measuring and interpreting charge dependent anisotropic flow, in: Proceedings, 24th International Conference on Ultra-Relativistic Nucleus-Nucleus Collisions, (Quark Matter 2014): Darmstadt, Germany, May 19–24, 2014, Nucl. Phys. A 931 (2014) 992–996, arXiv:1408.0714 [nucl-ex].
[33] Jaroslav Adam, et al., ALICE, Charge-dependent flow and the search for the chiral magnetic wave in Pb-Pb collisions at $\sqrt{s_{\rm NN}} = 2.76$ TeV, Phys. Rev. C 93 (2016) 044903, arXiv:1512.05739 [nucl-ex].
[34] Sang Eon Park, CMS, Charge asymmetry dependence of anisotropic flow in pPb and PbPb collisions with the CMS experiment, in: Proceedings, 26th International Conference on Ultra-Relativistic Nucleus-Nucleus Collisions, (Quark Matter 2017): Chicago, Illinois, USA, February 5–11, 2017, Nucl. Phys. A 967 (2017) 345–348, arXiv:1704.06712 [nucl-ex].
[35] Albert M. Sirunyan, et al., CMS, Probing the chiral magnetic wave in pPb and PbPb collisions at $\sqrt{s_{NN}} = 5.02$ TeV using charge-dependent azimuthal anisotropies, Phys. Rev. C 100 (2019) 064908, arXiv:1708.08901 [nucl-ex].
[36] L. Adamczyk, et al., STAR, Observation of charge asymmetry dependence of pion elliptic flow and the possible chiral magnetic wave in heavy-ion collisions, Phys. Rev. Lett. 114 (2015) 252302, arXiv:1504.02175 [nucl-ex].
[37] Qi-Ye Shou, STAR, Search for the chiral magnetic wave with anisotropic flow of identified particles at RHIC-STAR, in: Proceedings, 27th International Conference on Ultrarelativistic Nucleus-Nucleus Collisions, (Quark Matter 2018):

Venice, Italy, May 14–19, 2018, Nucl. Phys. A 982 (2019) 555–558, arXiv:1809.01980 [nucl-ex].
[38] Niseem Magdy, Shuzhe Shi, Jinfeng Liao, N. Ajitanand, Roy A. Lacey, New correlator to detect and characterize the chiral magnetic effect, Phys. Rev. C 97 (2018) 061901, arXiv:1710.01717 [physics.data-an].
[39] Niseem Magdy, Shuzhe Shi, Jinfeng Liao, Peifeng Liu, Roy A. Lacey, Examination of the observability of a chiral magnetically driven charge-separation difference in collisions of the $^{96}_{44}$Ru + $^{96}_{44}$Ru and $^{96}_{40}$Zr + $^{96}_{40}$Zr isobars at energies available at the BNL relativistic heavy ion collider, Phys. Rev. C 98 (2018) 061902, arXiv:1803.02416 [nucl-ex].
[40] Ling Huang, Mao-Wu Nie, Guo-Liang Ma, Sensitivity analysis of the chiral magnetic effect observables using a multiphase transport model, arXiv:1906.11631 [nucl-th], 2019.
[41] Niseem Magdy, Mao-Wu Nie, Guo-Liang Ma, Roy A. Lacey, A sensitivity study of the primary correlators used to characterize chiral-magnetically-driven charge separation, arXiv:2002.07934 [nucl-ex], 2020.
[42] Diyu Shen, Jinhui Chen, Guoliang Ma, Yu-Gang Ma, Qiye Shou, Song Zhang, Chen Zhong, Charge asymmetry dependence of flow and a novel correlator to detect the chiral magnetic wave in a multiphase transport model, Phys. Rev. C 100 (2019) 064907, arXiv:1911.00839 [hep-ph].
[43] Guo-Liang Ma, Bin Zhang, Effects of final state interactions on charge separation in relativistic heavy ion collisions, Phys. Lett. B 700 (2011) 39–43, arXiv:1101.1701 [nucl-th].
[44] Zi-Wei Lin, Che Ming Ko, Bao-An Li, Bin Zhang, Subrata Pal, A multi-phase transport model for relativistic heavy ion collisions, Phys. Rev. C 72 (2005) 064901, arXiv:nucl-th/0411110 [nucl-th].
[45] Guo-Liang Ma, Zi-Wei Lin, Predictions for $\sqrt{s_{NN}} = 5.02$ TeV Pb+Pb collisions from a multi-phase transport model, Phys. Rev. C 93 (2016) 054911, arXiv:1601.08160 [nucl-th].
[46] Guo-Liang Ma, Decomposition of the jet fragmentation function in high-energy heavy-ion collisions, Phys. Rev. C 88 (2013) 021902, arXiv:1306.1306 [nucl-th].
[47] Guo-Liang Ma, Medium modifications of jet shapes in Pb+Pb collisions at $\sqrt{s_{NN}}$ = 2.76 TeV within a multiphase transport model, Phys. Rev. C 89 (2014) 024902, arXiv:1309.5555 [nucl-th].
[48] Adam Bzdak, Guo-Liang Ma, Elliptic and triangular flow in p+Pb and peripheral Pb+Pb collisions from parton scatterings, Phys. Rev. Lett. 113 (2014) 252301, arXiv:1406.2804 [hep-ph].
[49] Mao-Wu Nie, Peng Huo, Jiangyong Jia, Guo-Liang Ma, Multiparticle azimuthal cumulants in p+Pb collisions from a multiphase transport model, Phys. Rev. C 98 (2018) 034903, arXiv:1802.00374 [hep-ph].
[50] Xin-Nian Wang, Miklos Gyulassy, HIJING: a Monte Carlo model for multiple jet production in pp, pA and AA collisions, Phys. Rev. D 44 (1991) 3501–3516.
[51] Miklos Gyulassy, Xin-Nian Wang, HIJING 1.0: a Monte Carlo program for parton and particle production in high-energy hadronic and nuclear collisions, Comput. Phys. Commun. 83 (1994) 307, arXiv:nucl-th/9502021 [nucl-th].
[52] Bin Zhang, ZPC 1.0.1: a parton cascade for ultrarelativistic heavy ion collisions, Comput. Phys. Commun. 109 (1998) 193–206, arXiv:nucl-th/9709009 [nucl-th].
[53] Bao-An Li, Che Ming Ko, Formation of superdense hadronic matter in high-energy heavy ion collisions, Phys. Rev. C 52 (1995) 2037–2063, arXiv:nucl-th/9505016 [nucl-th].
[54] Guo-Liang Ma, Final state effects on charge asymmetry of pion elliptic flow in high-energy heavy-ion collisions, Phys. Lett. B 735 (2014) 383–386, arXiv:1401.6502 [nucl-th].
[55] Jurgen Schukraft, Anthony Timmins, Sergei A. Voloshin, Ultra-relativistic nuclear collisions: event shape engineering, Phys. Lett. B 719 (2013) 394–398, arXiv:1208.4563 [nucl-ex].
[56] Shreyasi Acharya, et al., ALICE, Constraining the magnitude of the chiral magnetic effect with event shape engineering in Pb-Pb collisions at $\sqrt{s_{NN}}$ = 2.76 TeV, Phys. Lett. B 777 (2018) 151–162, arXiv:1709.04723 [nucl-ex].
[57] Jie Zhao, Search for the chiral magnetic effect in relativistic heavy-ion collisions, Int. J. Mod. Phys. A 33 (2018) 1830010, arXiv:1805.02814 [nucl-ex].